Performance of the GSN station DAV-IU, 1994-2009

A report in a series documenting the status of the Global Seismographic Network

WQC Report 2010:7
February 5, 2010

Göran Ekström and Meredith Nettles

Waveform Quality Center
Lamont-Doherty Earth Observatory of Columbia University, New York

1 Station performance report: DAV

This report summarizes a number of observations that are relevant for assessing the past and current quality of the data recorded at one of the stations of the Global Seismographic Network. The purpose of the report is, in part, to document specific problems observed with the data. Some of these problems are related to errors in the available descriptions of station parameters: orientation of the sensors, response functions, polarities. In principle, such errors in the station metadata can be corrected by providing updated station parameters. In practice, this may be difficult in some cases due to lack of knowledge of, or inability to determine, the correct parameters. Other problems are caused by the malfunctioning of some instrument component. Regardless of the cause, it is necessary to document and publicize the lack of accurate and reliable station characteristics, especially when it is not obvious from simple inspection of the data that a problem exists. It is also of value to document the characteristics of stations performing well, both to establish their high quality and to help identify installation and operation procedures that should be emulated at other stations.

1.1 Station DAV

The station DAV (Davao) is located in the city of Davao on the island of Mindanao, southeastern Philippines (Figure 1). The station is located in an area of intense seismicity and complex tectonics. The closest GSN station is KAPI-II (Kappang), located approximately 1500 km to the southwest.

DAV is part of the USGS (IU) component of the IRIS/USGS Global Seismographic Network.

1.2 The data

Digital seismic data from DAV are available from the IRIS DMC beginning in 1994. Here, we consider broadband instruments at the station. The initial installation consisted of a set of STS-1 seismometers. An auxiliary STS-2 seismometer was installed in 2007. Data from DAV are considered in our standard CMT analysis (Dziewonski et al., 1981; Ekström et al., 2005), and waveform data, travel-time observations, and dispersion curves derived from DAV data have been used in the development of global and regional tomographic models since the station was installed.

In the analyses described here, we have made use of data collected from the IRIS DMC. We requested and downloaded all long-period (LH) and very-long-period (VH) data available at the DMC for both sensors

from the start of operation (1994) until August 2009. We used the currently available station metadata prepared by the Albuquerque Seismological Laboratory and available at the IRIS DMC (downloaded in December 2009). Overall, the station has been operated with few data outages since 1994.

1.3 The metadata

The dataless SEED volume for DAV documents 4 response epochs for the STS-1 (primary) and STS-2 (secondary) sensors. The STS-1 1 sps channels were initially called LHZ, LHN, LHE, without a location code. They were renamed with the location code 00 on 1999.092 (092 representing the julian day). We refer to these channels as LHZ-00, LHN-00, and LHE-00. The STS-2 sensor (location code 10) was installed on 2007.083, and we refer to the 1 sps channels as LHZ-10, LHN-10, and LHE-10. Epoch boundaries are given at 1994.352 (first STS-1 data), 1997.318, 1999.092, 1999.110, 1999.130, 2007.083 (first STS-2 data), and 2009.173. The metadata indicate no changes in gain or frequency characteristics of the two sensors during the period 1994–2009.

1.4 Scaling analysis

One method for assessing the quality of the data is the systematic comparison of recorded long-period waveforms with synthetic seismograms calculated for known seismic events. This analysis follows the steps described by Ekström et al. (2006). Seismic data for the LH and VH channels from both the STS-1 and STS-2 sensors are collected. Corresponding synthetic waveforms for all earthquakes in the Global CMT catalog (Dziewonski et al., 1981; Ekström et al., 2005) with $M_W \geq 6.5$ are calculated. Correlation coefficients and optimal scaling factors between observed and synthetic waveforms are calculated for the three types of data used in the standard CMT analysis: body waves (B), with periods in the range 50–150 sec, mantle waves (M), with periods in the range 125–350 sec, and surface waves (S), with periods in the range 50–150 sec. Body- and mantle-wave results are discussed here. The scaling factor is only calculated for waveforms with a correlation of 0.75 or greater. The scaling factor is the number by which the synthetic seismogram should be multiplied to maximize the agreement with the observed seismogram. Annual median values of the scaling factors are calculated when four or more individual event scaling estimates are available for the year. Reversed components can be identified by their large negative correlations.

Figure 2 shows the results of our systematic comparison of DAV waveforms with synthetic seismograms. The diagram illustrates several problems with the data. Good correlation of all three components of the primary sensor with synthetic waveforms is only seen in 1995. Starting in early 1996, slightly more than one year after installation, the E–W component no longer matches the synthetics, and the the fits for the vertical and N–S components change in a similar way during 1996 and 1997. During the period 1998–2006, only a very small number of body-wave seismograms correlate well enough with model waveforms to allow a scaling factor to be calculated. The problem is worse for mantle waves. The scaling factors all indicate significant loss of gain.

Coincident with installation of the STS-2 in 2007, the quality of the STS-1 vertical and N–S waveforms improved, but then deteriorated rapidly once again. The STS-1 E–W waveforms did not improve. The STS-2 has generated seismograms that correlate sufficiently well with the synthetic waveforms to allow scaling factors to be calculated, although the horizontal components have not generated enough measurements in the mantle-wave period band to result in the calculation of annual median scaling factors.

1.5 Noise analysis

A second method for investigating the overall performance of the sensors is to monitor background noise levels for all seismic channels, after conversion of the data to ground acceleration. We calculate hourly rms

values of the time-domain seismic signal in narrow frequency bands, and convert the rms values to a power spectral density (PSD) at that frequency using Parseval's theorem. For each month, we then calculate the low-noise value at each frequency by determining the PSD amplitude not exceeded 10% of the time.

The PSD data provide much information about the station and the sensors. Figure 3 shows the monthly low-noise estimate for each LH channel at 72 s period since 1994. The first observation is that the station has provided data without any major outages since 1994. The second observation is that the noise levels for the STS-1 seismometers have been highly variable throughout the period of operation. Some of the largest changes are associated with response epoch boundaries. The STS-2 noise levels have been relatively constant, but very high. They are $\sim$15 dB higher than those recorded on the STS-1 during 1995, when the STS-1 sensor appears to have been operating properly (Figure 2).

1.6 Inter-sensor coherence

An additional method for assessing the quality and calibration of the recorded signals is to calculate inter-sensor coherence. This analysis is possible when more than one sensor is operated in the same location. At DAV, this is possible for the period 2007-2009, during which time both STS-1 and STS-2 instruments have been operating.

We calculate the coherence of the deconvolved vertical, N–S, and E–W components. The coherence is calculated for $\sim$2-hour-long time windows containing the signals for earthquakes with $M_W \geq 6.5$ (the same events used in the scaling analysis). For each pair of seismograms, the coherence is calculated in narrow frequency bands around 32 s, 64 s, 128 s and 256 s. If the coherence is greater than 0.95, the value is stored together with the complex scaling factor (represented here as a scaling factor and phase shift) that should be applied to the secondary-sensor data to bring the two time series into the best agreement. In the following, the discussion is based on the initial assumption that the secondary (STS-2) sensor is properly calibrated and that deviations from a scaling factor of 1.0 and a phase shift of 0° should be attributed to differences between the true and reported response functions of the primary (STS-1) sensor.

Figure 4 shows the results of the coherence analysis for the vertical component. The agreement between the two instruments has never been good. The STS-1 displays a significant loss of long-period gain and a corresponding phase shift. The loss of gain is time variable, with two periods of gradual loss of gain and a sudden limited recovery in late 2007. We interpret the deviations as problems with the STS-1, since the scaling analysis shows that the STS-2 signal remains in agreement with the synthetic seismograms (Figure 2).

Figure 5 shows the amplitude and phase differences for the N–S components. The agreement between the signals is never good, and the STS-1 displays a loss of long-period gain and corresponding phase shifts during the entire period.

Figure 6 shows the results for the E–W component. The STS-1 response is incorrect, with the gain at 32-s period reduced by a time-varying factor of 0.2–0.4, with larger gain losses at longer periods. The phase response is in error by more than 60° at 32 s.

1.7 Polarization analysis

The orientation of the horizontal components can be assessed empirically by comparing observed and synthetic waveforms, and finding the angle by which the horizontal components should be rotated in order to maximize the agreement. We follow the approach described by Ekström and Busby (2008) for such a comparison, using the observed and synthetic waveforms from Global CMT analysis.

We apply the method of Ekström and Busby (2008) to the same dataset used in the scaling analysis. Figure 7 shows the individual measurements for the period of operation for the different channels. Overall, the number of useful observations for the STS-1 sensor is small and all derive from the period 1994–1997, a consequence of the malfunctioning horizontal components. The STS-2 has generated a number of measurements since its installation in 2007, but the scatter in these measurements is quite large. The median estimates for the entire period of operation are given in Table 1. In general, the scatter is such that the it is difficult to assess whether the observations are consistent with the orientations provided in the metadata. The earliest STS-1 data (1995–1996) appear consistent with the metadata (Figure 7).

Comp. 1	Comp. 2	First	Last	# Obs.	N	Az 1	Az 2	25%	Med.	75%
LHE	LHN	19941228	19990328	173	20	90	0	-8	-4	6
LHE-00	LHN-00	19990403	20090830	422	0	90	0	-	-	-
LHE-10	LHN-10	20070325	20090830	121	29	90	0	-14	-4	2

Table 1: Statistics of sensor-rotation angles estimated in this study. Columns are the channel names, the dates of the first and last observations considered in making the estimate, the total number of observations, the number of observations of acceptable quality, the reported azimuths of sensitivity of the two channels, the median polarization-angle deviation from the reported orientation together with the range of the second (25%) and third (75%) quartiles of the observations. No measurements were possible for the STS-1 sensor after 1999 (channels LHE-00, LHN-00).

1.8 Example seismograms

The anomalies described here agree with observations we have made in our routine analysis of waveforms for the determination of CMT earthquake parameters. When confronted with the seismograms for an individual earthquake, it is often difficult to assess whether a poor fit is due to incorrect source parameters, inadequate modeling of wave propagation through an Earth model, or some problem with the recorded seismograms. Here, we have included some examples of data that illustrate the characteristics of the types of problems that we have encountered with data from the DAV station.

Figure 8 shows an example of three-component STS-1 mantle-wave data for an earthquake on May 27, 1995, approximately 6 months after the station was installed. All components are well fit, reflecting the general health of the station during its first year of operation.

Figure 9 shows a comparison between observed and synthetic body- and mantle-wave seismograms for an earthquake on November 28, 1997. By this time, a general deterioration of the STS-1 sensor is obvious in both period bands. Body waves on the vertical and E–W components are severely misfit, and all mantle-wave components show gross differences between observed and synthetic waveforms.

The top panel of Figure 10 shows a comparison of mantle-wave seismograms recorded on the STS-1 seismometer and the corresponding synthetic waveforms for an event on August 15, 2007, five months after the auxiliary STS-2 was installed at the station. The behavior of the STS-1 is similar to that illustrated in Figure 9: dramatic loss of gain at long periods, with corresponding phase shifts. The bottom panel shows the STS-2 seismograms. The fit is generally good. The Love waves are nearly nodal, and the G2 arrival is nearly absent, presumably a consequence of refraction or defocusing.

Figure 11 shows STS-1 and STS-2 surface-wave seismograms for an $M_W = 7.5$ earthquake on August 10, 2009. The frequency response for the STS-1 seismograms (top panel) is grossly incorrect, especially for the E–W component. The STS-2 seismograms (bottom panel) are adequately fit. A slight phase shift is mostly a consequence of source finiteness. Intermediate-period surface waves would normally not be used in

our CMT analysis for an earthquake of this size, but noise levels at the site preclude the use of longer-period data.

2 Summary and analysis

At the time of writing (February, 2010), the STS-1 sensor at the GSN station DAV is essentially broken. No component is recording well-calibrated ground-motion data. The auxiliary sensor is recording calibrated data, but very high noise levels (Figure 3) limit its utility.

The vertical and horizontal STS-1 seismometers are malfunctioning and have been malfunctioning since 1997. A severe loss of long-period gain has affected all three components since shortly after installation (Figure 2), and time-dependent variations of the responses are also evident (Figure 4–6). No useful data have been recorded by the STS-1 sensor since 1997.

The STS-2 sensor has generated good data for large earthquakes since installation (Figure 10 and Figure 11). Very high noise levels, especially on the horizontal components, limit the utility of the auxiliary STS-2 sensor.

3 Conclusions and recommendations

This analysis shows that DAV generated data potentially of GSN quality only for the first year or two of operation. The station has suffered from a chronic STS-1 sensor problem since 1997, a period of more than 10 years. Unfortunately, the magnitude and variability of the errors make it unlikely that any retroactive remedy for the observed problems will be possible.

The sensor problems described here should have been identified early on, and corrected. We speculate that the problem went unnoticed or undiagnosed because no routine calibrations are performed at GSN stations. The lack of systematic calibrations, and inspection of calibration results, makes it difficult to identify instrument problems. In addition, the lack of calibrations makes it nearly impossible to repair errors in instrument parameters once a problem has been identified. The symptoms of the STS-1 malfunction are similar to those observed at other stations (Ekström et al., 2006; Ekström and Nettles, WQC Report 2010:6); interpretation is complicated by the presence of multiple sensor problems.

Modern seismological analyses require well-calibrated instruments. Amplitude variations of 10% and smaller are interpreted as signals in modern studies that seek to map the attenuating properties of the Earth's interior (e.g., Dalton and Ekström, 2006). Phase anomalies of a few seconds at long periods are similarly interpreted in terms of Earth's elastic structure by numerous authors. Data from DAV have been used in such studies with the assumption that the station is meeting GSN design goals (IRIS, 1985; Lay et al., 2002) with respect to instrument stability. Clearly it does not, and its failure to do so should be documented. This is particularly important when, as for DAV, the data may at times appear visually to be correct, but are actually faulty.

We urge restoration of DAV to a state where it generates GSN-quality data. It is unfortunate that the secondary data stream provided by the STS-2 is so noisy. It would be fruitful to determine whether an improved installation of the STS-2 could lower the noise levels. The quality of the data recorded on the STS-1 sensor soon after installation (1994–1996) indicates that, at least at that time, it was possible to achieve significantly lower noise levels than those exhibited by the current STS-2 installation.

4 References

Dalton, C. A., and G. Ekström, Global models of surface wave attenuation, *J. Geophys. Res.*, 111, B05317, 2006.

Dziewonski, A. M., T.-A. Chou, and J. H. Woodhouse, Determination of earthquake source parameters from waveform data for studies of global and regional seismicity, *J. Geophys. Res.*, 86, 2825–2853, 1981.

Ekström, G., A. M. Dziewonski, N. N. Maternovskaya, and M. Nettles, Global seismicity of 2003: Centroid-moment tensor solutions for 1087 earthquakes, *Phys. Earth Planet. Inter.*, 148, 327–351, 2005.

Ekström, G., C. A. Dalton, and M. Nettles, Observations of time-dependent errors in long-period gain at global seismic stations, *Seism. Res. Lett.*, 77, 12–22, 2006.

Ekström, G., and R. W. Busby, Measurements of seismometer orientation at USArray Transportable and Backbone stations, *Seism. Res. Lett.*, 79, 554-561, 2008.

Ekström, G., and M. Nettles, Performance of the GSN station WCI-IU, 1997–2009, Waveform Quality Center Report 2010:6, 2010.

IRIS, *The design goals for a new global seismographic network*, IRIS GSN committee report, 31 pages, 1985.

Lay, T., J. Berger, R. Buland, R. Butler, G. Ekström, B. Hutt, B. Romanowicz, *Global seismic network design goals update 2002*, IRIS GSN committee report, 2002.

Nettles, M., and G. Ekström, Glacial earthquakes in Greenland and Antarctica, *Annual Reviews*, in review, 2010.

Peterson, J., Observations and modeling of background seismic noise, *U. S. Geol. Surv. Open-file Rep. 93-322*, 1–45, 1993.

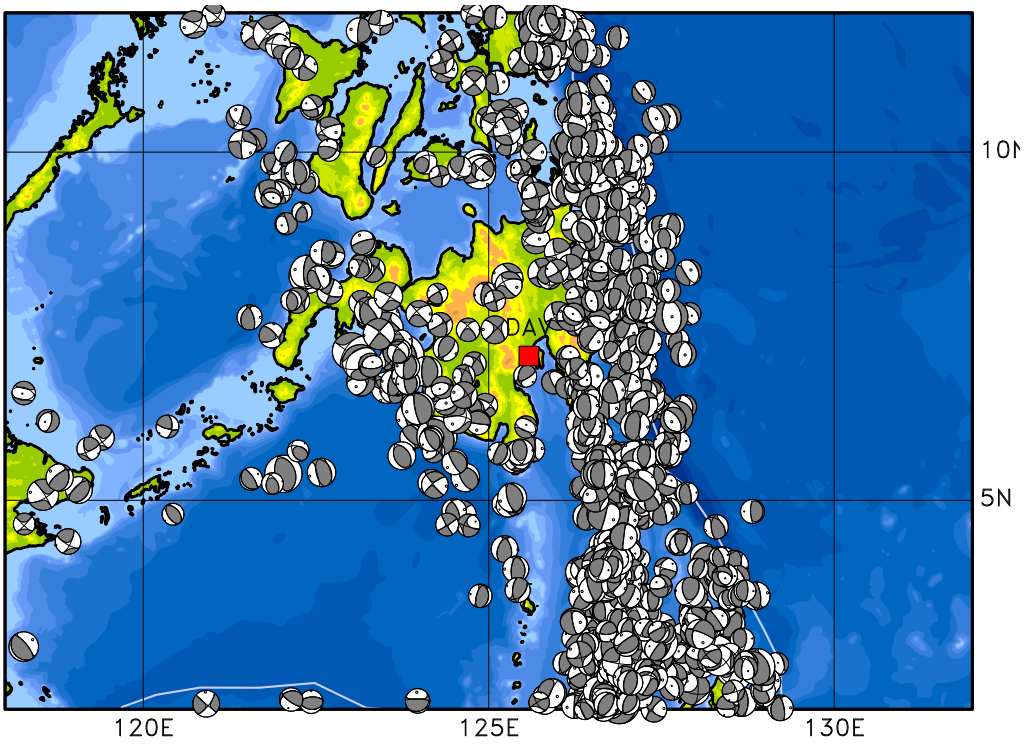

Figure 1: Map showing the location of DAV (red square in the center). Grey focal mechanisms show earthquake locations and moment tensors from the Global CMT catalog. The closest GSN station is KAPI-II, located 1500 km to the southwest of DAV.

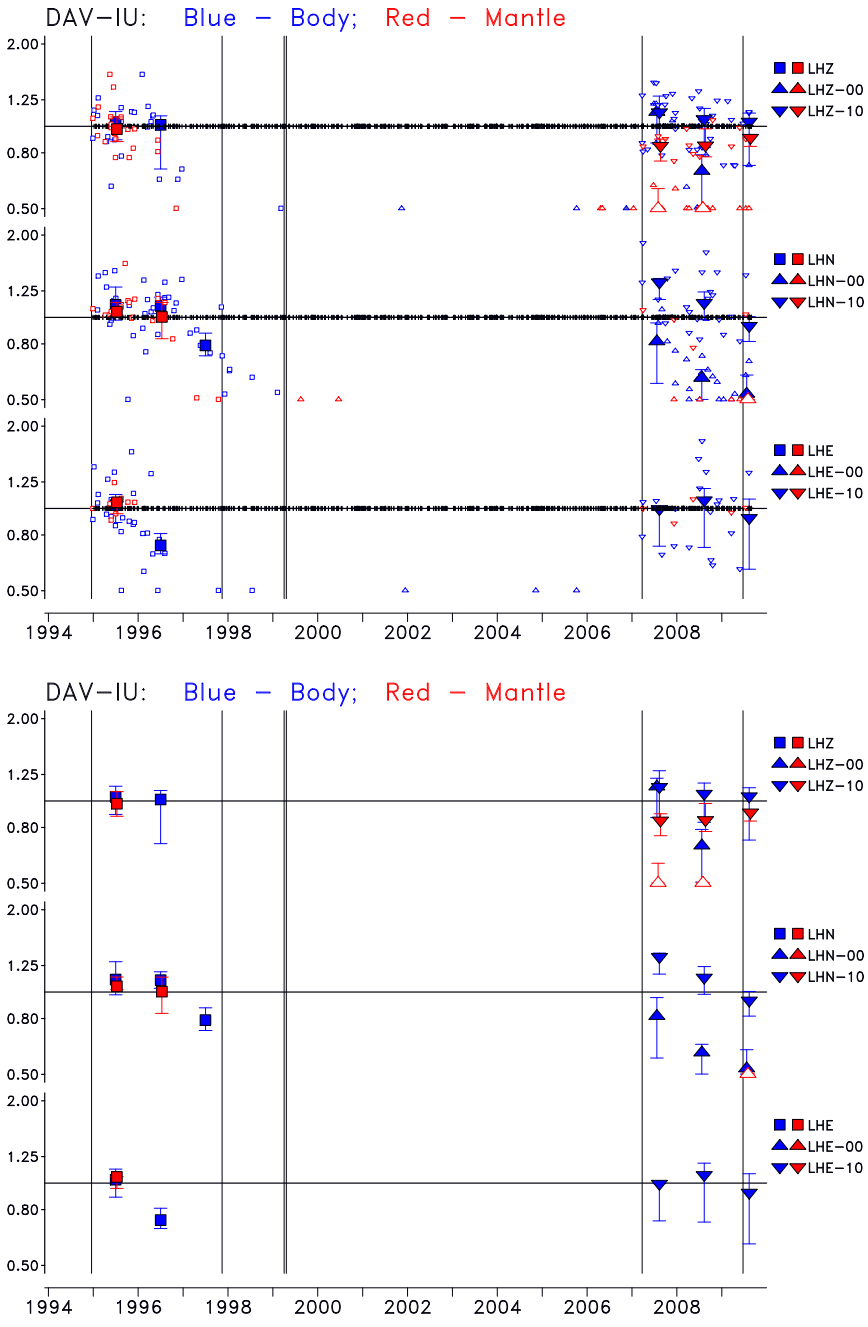

Figure 2: Scaling factors for the data channels at DAV. Small symbols in top panel show scaling factors for individual traces. Tick marks on the horizontal axes show times of observations for which the correlation was less than 0.75. Large symbols show the median scaling factor for each year, with the error bars corresponding to the range of the second and third quartiles of the scaling factors. The legend on the right identifies the symbol type with a specific channel. Open large symbols indicate that the annual scaling factor was smaller than 0.5. Thin vertical lines show the response epoch boundaries present in the metadata. Bottom panel shows only the annual median values. No scaling measurements were possible during 1998–2006.

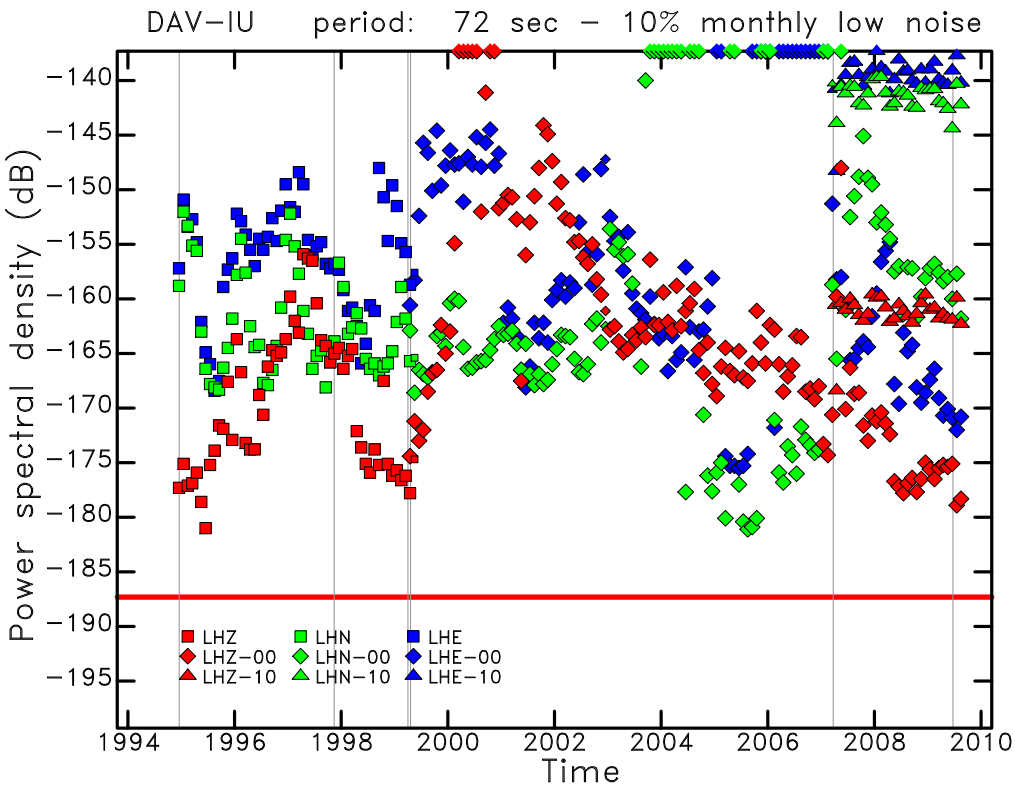

Figure 3: Diagram shows the monthly PSD of ground acceleration at 72-s period for all long-period (LH) channels at DAV for the period 1994–2009. Smaller symbols are used for months with fewer available hourly measurements. Each component and sensor is represented by a distinct symbol and color. The red horizontal line indicates the level of Peterson's (1993) Low Noise Model (LNM) at 72 s. The thin vertical lines show the times of epoch boundaries in the station metadata. Observed noise levels are erratic; some, but not all, of the largest changes are associated with epoch boundaries. The STS-2 noise levels are stable, but very high.

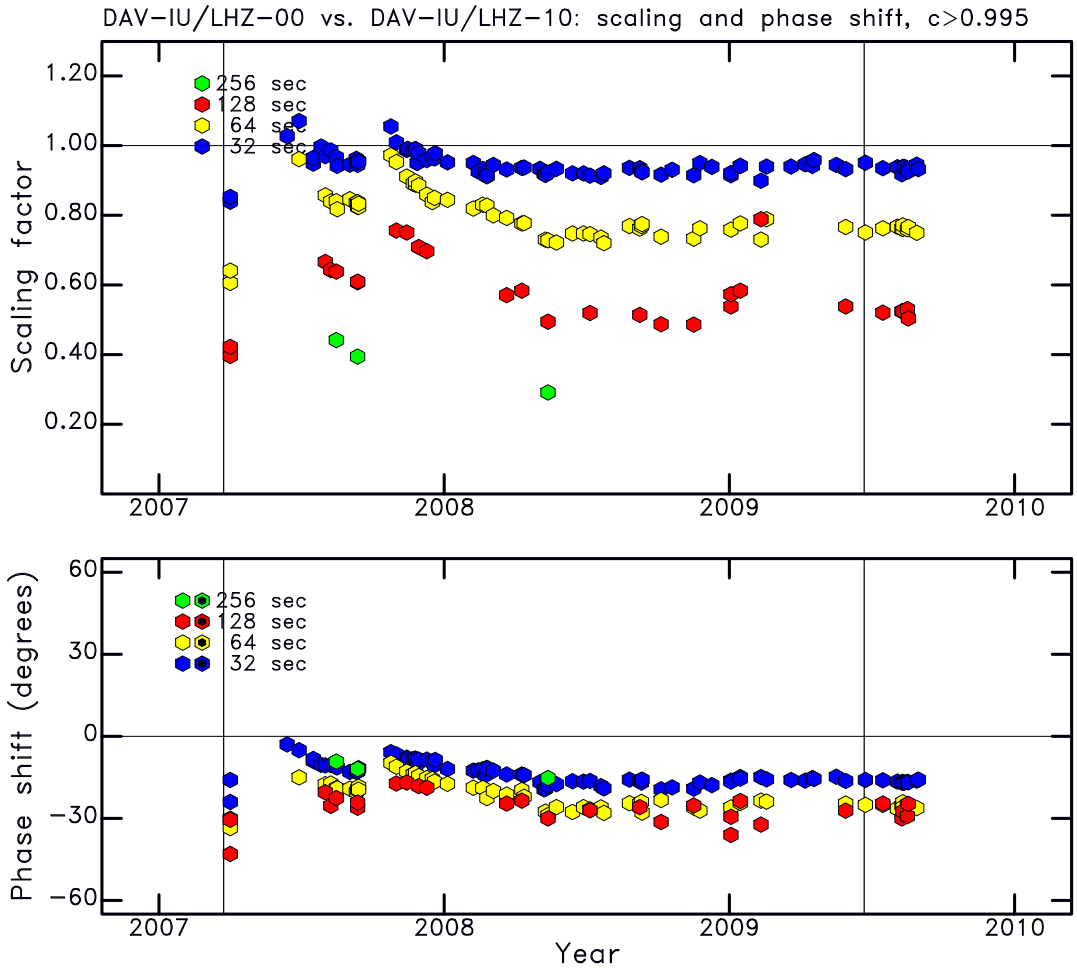

Figure 4: Diagram shows the result of coherence analysis for the vertical components of the STS-1 and STS-2 sensors. Each symbol represents a measurement of coherence for a $M_W \geq 6.5$ earthquake. The minimum coherence plotted is indicated by c. The scaling factor and phase shift between the two time series is shown at four periods. The STS-1 long-period response is never good, exhibiting both gradual and abrupt changes. The thin vertical lines show the times of epoch boundaries in the station metadata.

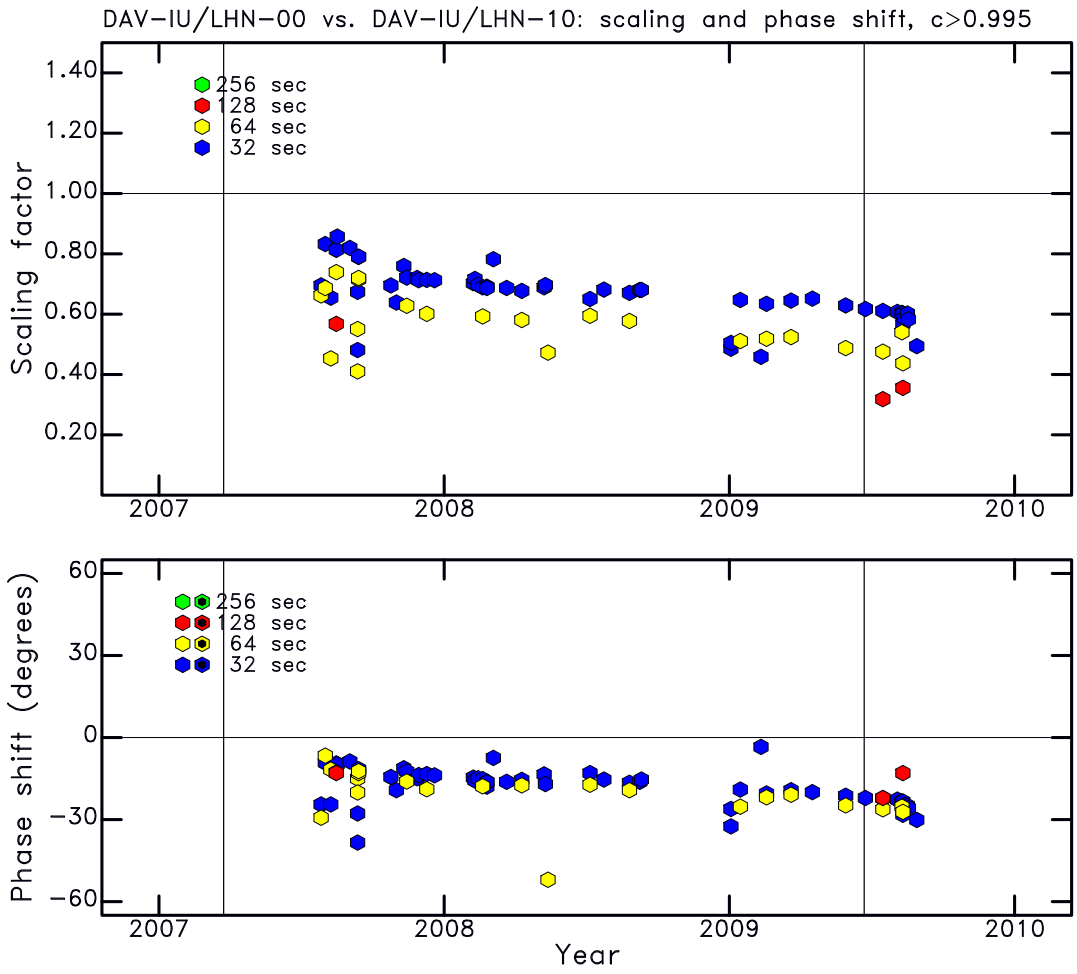

Figure 5: Same as Figure 4, but for the North-South components. The responses of the two instruments are grossly different, and the long-period gain of the STS-1 deteriorates during 2007–2009.

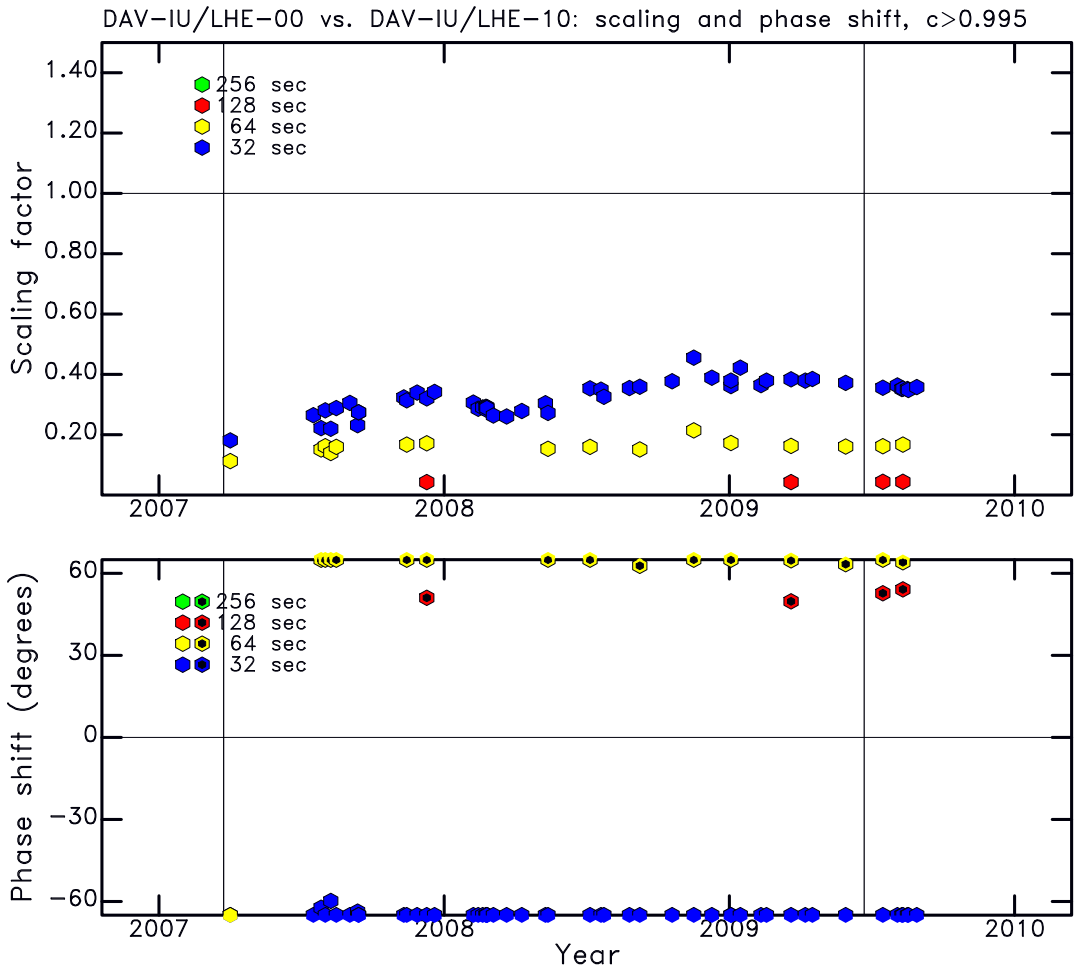

Figure 6: Same as Figure 4, but for the East-West components. The problems on the East-West component are similar to those on the North-South component, but the deviations are larger. The STS-1 gain varies with time, and the phase error is $> 60°$ at a period of 32 s. A black dot in the symbol indicates a phase shift in addition to a $180°$ phase shift.

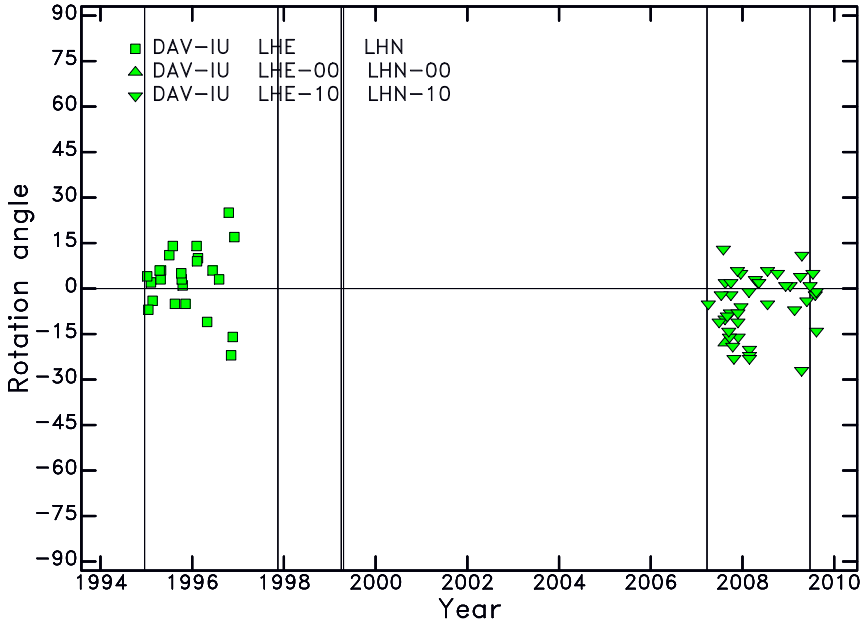

Figure 7: Individual measurements of polarization angle as a function of time. All measurements for the period of operation are shown. Symbols represent measurements obtained in the surface-wave band of the CMT analysis. The thin vertical lines show the times of epoch boundaries in the station metadata.

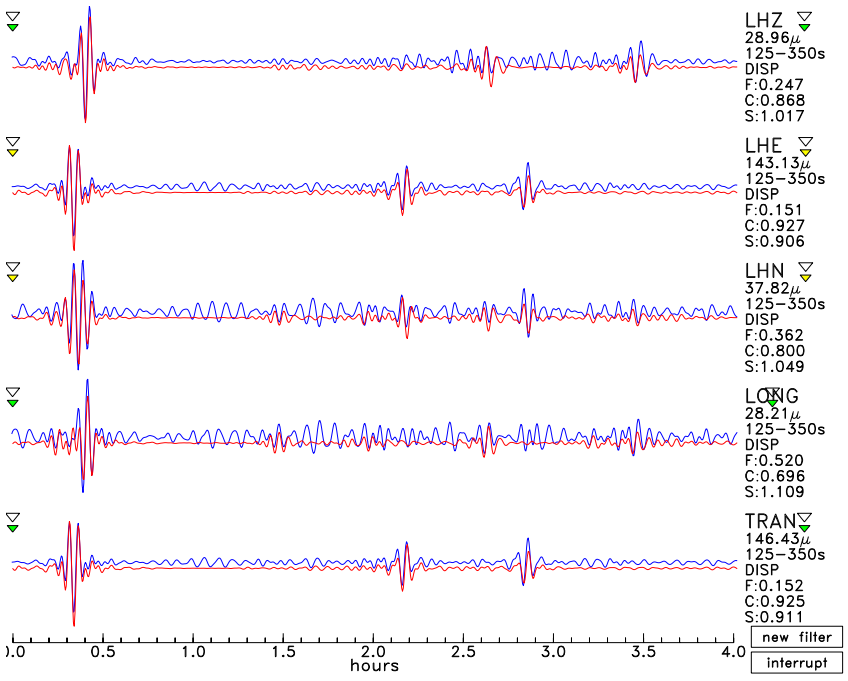

Figure 8: Comparison of observed (blue traces) and synthetic (red traces) mantle-wave seismograms recorded on the STS-1 sensor for a $M_W = 7.0$ earthquake on May 27, 1995. The channel name, maximum displacement, and values for the three parameters residual misfit (F), correlation (C) and scaling factor (S) are given to the right of each waveform. All channels are well fit.

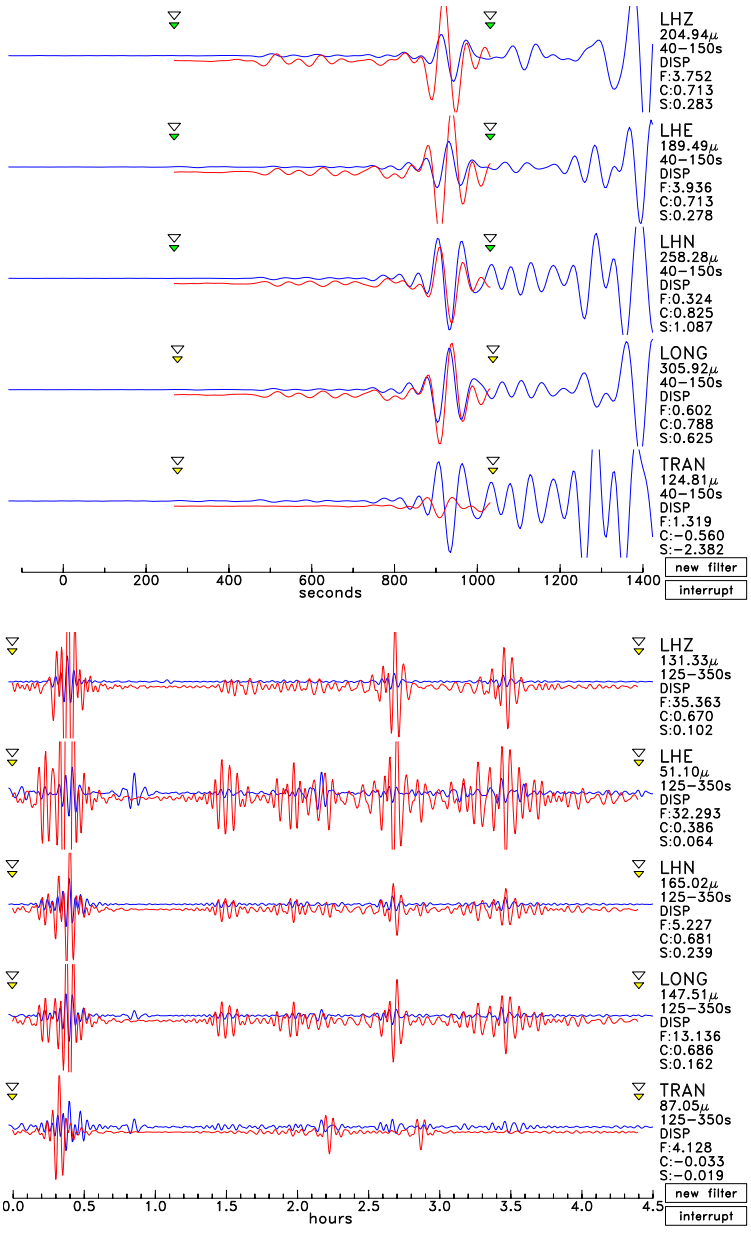

Figure 9: (Top) Observed (STS-1) and synthetic body-wave seismograms for a $M_W = 7.5$ earthquake on November 8, 1997. The vertical and E–W components are poorly fit, reflecting errors in the response functions. The problem is not simply a difference in gain. (Bottom) Observed and synthetic mantle-wave seismograms for the same earthquake. The response at long periods is incorrect, with an amplitude error larger than a factor of 10 for the E–W component.

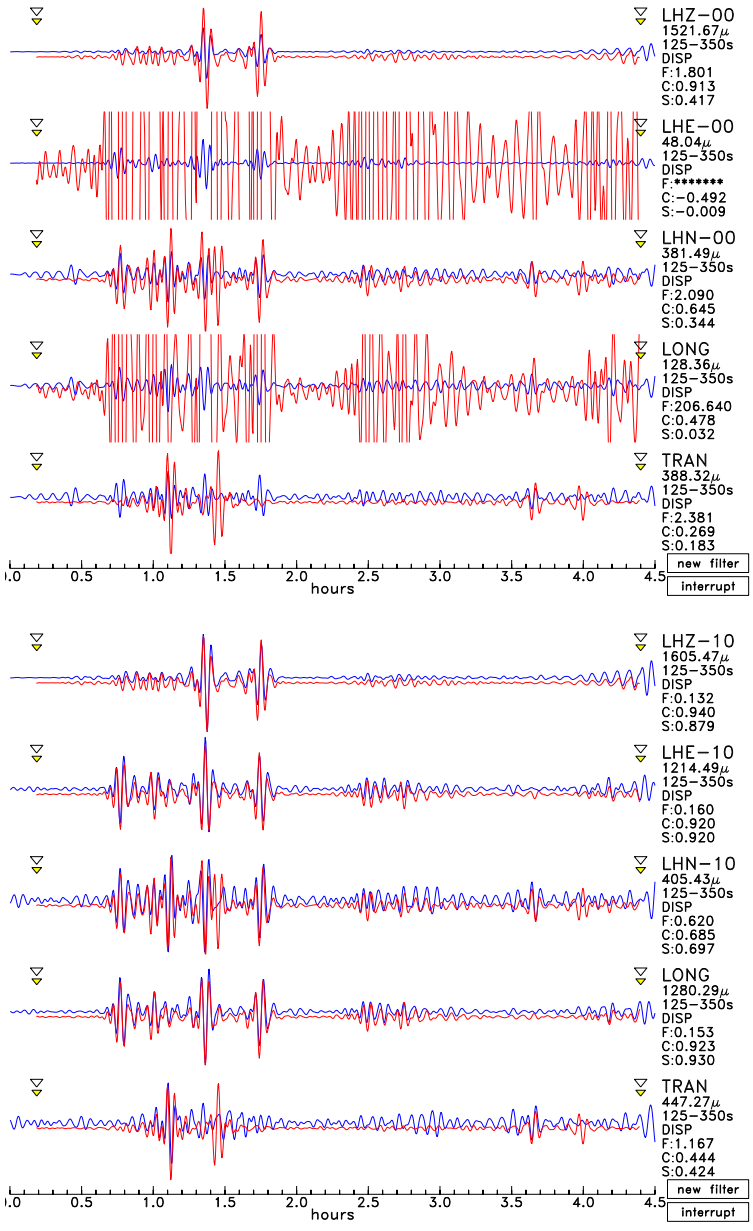

Figure 10: (Top) Observed (STS-1) and synthetic mantle-wave seismograms for an earthquake on August 15, 2007. The responses for the vertical and N–S components are incorrect, reflecting loss of gain at long periods. The E–W component is suffering even more severe problems. (Bottom) Observed (STS-2) and synthetic body-wave seismograms for the same earthquake. The fit is good on all components.

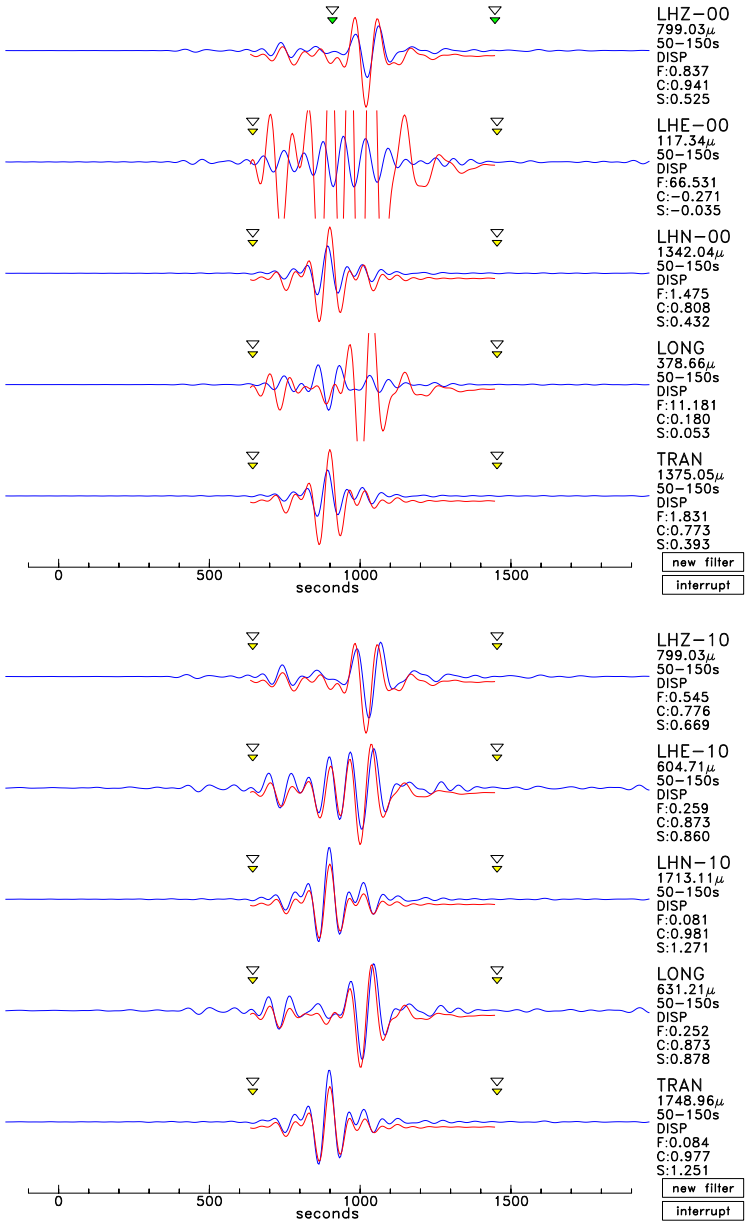

Figure 11: (Top) Observed (STS-1) and synthetic surface-wave seismograms for an $M_W = 7.5$ earthquake on August 10, 2009. The E–W component shows a grossly incorrect frequency response. The responses for the vertical and N–S components are also incorrect. The problem is not simply a difference in gain. (Bottom) Observed (STS-2) and synthetic surface-wave seismograms for the same earthquake, but recorded on the STS-2 seismometer. The fit is adequate on all components. The observed phase shifts are likely due to source-finiteness effects.